

# Comparing resource requirements of noisy quantum simulation algorithms for the Tavis–Cummings model

Alisa Haukisalmi<sup>1</sup>, Matti Raasakka<sup>1</sup>, and Ilkka Tittonen<sup>1</sup>

<sup>1</sup>Micro and Quantum Systems research group, Department of Electronics and Nanoengineering, School of Electrical Engineering, Aalto University

## Abstract

Fault-tolerant quantum computers could facilitate the simulation of quantum systems unfeasible for classical computation. However, the noisy intermediate-scale quantum (NISQ) devices of the present and near term are limited and their utilisation requires additional strategies. These include quantum error mitigation (QEM) for alleviating device noise, and variational quantum algorithms (VQAs) which combine classical optimization with short-depth, parameterized quantum circuits. We compare two such methods: zero-noise extrapolation (ZNE) with noise amplification by circuit folding, and incremental structural learning (ISL), a type of circuit recompiling VQA. These are applied to Trotterized time-evolution of the Tavis–Cummings model (TCM) under a noise simulation. Since both methods add circuit evaluation overhead, it is of interest to see how they compare both in the accuracy of the dynamics they produce, and in terms of the quantum resources used. Additionally, noisy recompilation of time-evolution circuits with ISL has not previously been explored. We find that while ISL achieves lower error than ZNE for smaller system sizes, it fails to produce correct dynamics for 4 qubits, where ZNE is superior. Diverging resource requirements for ISL and ZNE are observed, with ISL achieving low circuit depths at the cost of a large number of circuit evaluations.

## 1 Introduction

With potential applications ranging from materials science [1, 2] to lattice gauge theories [3], efficient simulation of quantum mechanical systems with quantum computers is of great interest. The motivation for using quantum computers arises from the dimensions of quantum mechanical systems which increase exponentially in the degrees of freedom, making classical simulations impossible for larger systems. The idea of bypassing this exponential problem by using a quantum mechanical system itself to simulate quantum dynamics was proposed by Feynman in 1982 [4], and later, in 1996 [5], Lloyd showed that the time-evolution of local Hamiltonians can indeed be efficiently simulated by an application of the Trotter product formula [6]. This approach, also known as Trotterization, has become the standard method of simulating Hamiltonian evolution on digital quantum computers [7, 8].

Present-day quantum computers are, however, not able to run arbitrary circuits: They are limited in their qubit number and connectivity, and suffer from significant noise. Because the

depth of a Trotterized time-evolution circuit increases linearly in the number of time steps, these so-called noisy intermediate-scale quantum (NISQ) machines [9] require additional strategies for quantum simulation. Quantum error mitigation (QEM) methods such as zero-noise extrapolation (ZNE) [10] or probabilistic error cancellation (PEC) [11, 12] can be used to alleviate the effect of noise on computations. An alternative though not conflicting approach is to use variational quantum algorithms (VQAs) [13, 10], which combine classical optimization with parameterized, low-depth quantum circuits.

QEM can be applied to time-evolution to improve the expectation values measured from the Trotterized circuits. However, if the circuit becomes too deep and hence the noise too severe, QEM will be of little use. VQAs can either completely bypass Trotterization, for example, by methods based on evolving a parameterized trial state [14, 15], or they may attempt to recompile the Trotter circuits into shorter approximations [16, 17]. These methods come with their drawbacks as well, since the resource cost of classical optimization and the increased number of circuit evaluations can erase the benefits of using VQAs.

We compare the performance of two kinds of time-evolution algorithms applied to Tavis–Cummings systems [18] of varying size. The two algorithms are Trotterization with ZNE, and a time-evolution application of incremental structural learning (ISL) [16], a type of circuit recompiling VQA. Trotterization has been compared to other time-evolution VQAs [19] and specifically to ISL as well [20], and as stated, suffers from linearly increasing circuit depths, while ISL trades depth for circuit evaluations. Since ZNE adds evaluation overhead to Trotterization as well, it is of interest to compare how it and ISL perform in terms of quantum resources used, and under noisy conditions. Time-evolution with ISL where the recompilation itself is done under noise has also not been previously reported on.

This paper is structured such that Section 2.1 describes the time-evolution methods under comparison, and the Tavis–Cummings model system is presented in Section 2.2. Details about the circuit simulations are given in Section 2.3, and Section 2.4 is on estimating the circuit evaluations required by the algorithms. The simulation results are presented and discussed in Section 3, and Section 4 presents a summary of the work.

## 2 Methods

### 2.1 Time-evolution methods

Given a qubit Hamiltonian  $H$  and an initial state  $|\phi_0\rangle \equiv |\phi(0)\rangle$ , the state of the system at a later time  $t$  can be found as  $|\phi(t)\rangle = U(t)|\phi_0\rangle$ , where  $U(t) = e^{-iHt}$  is the time-evolution operator. To simulate the time-evolution of the system,  $U(t)$  must be implemented as a set of common gates. As the basis for our comparisons we use Trotterization, and the other two methods are based on improving the Trotterized circuits.

#### 2.1.1 Trotterization

Given a qubit Hamiltonian  $H = \sum_{k=1}^L H_k$  whose terms all commute with each other, the time-evolution operator is simply  $\exp(-iHt) = \prod_k \exp(-iH_k t)$ . Additionally, if each term is a Pauli string, i.e. a tensor product of Pauli operators (including  $\mathbb{I}$ ), the factors  $\exp(-iH_k t)$  have known decompositions in terms of standard gates [7] and  $U(t)$  can be implemented. In the general case where  $[H_k, H_l] \neq 0$  for some  $k, l$ , the time-evolution operator can still be approximated by the

above product by applying the Trotter product formula, resulting in [5]

$$e^{-iHt} = \left( \prod_{k=1}^L e^{-iH_k t/N_T} \right)^{N_T} + O(t^2/N_T). \quad (1)$$

This is with the additional assumption that each of the  $L$  terms is local, meaning that the terms act on at most a constant number of qubits, and that  $L$  is polynomial with respect to  $N_q$ , the number of qubits.

This application of the Trotter product formula can be concisely referred to as Trotterization [21, 22, 23], and we refer to  $N_T$  as the number of Trotter steps. By defining  $\Delta t \equiv t/N_T$  as the simulation time step and  $T \equiv \prod_k \exp(-iH_k \Delta t)$  as the Trotter step, we may simulate each time step  $n = 0, 1, \dots, N_T$  by applying  $U(n\Delta t) \approx T^n$ .

### 2.1.2 Error-mitigated Trotter steps

The linearly growing depth of the Trotterized time-evolution circuits poses a challenge for NISQ devices, and QEM subroutines can be used to improve these noisy measurement results: Given a quantum circuit  $U$  and some observable of interest  $M$ , QEM aims to mitigate the error of the expectation value  $\langle M \rangle \equiv \langle \mathbf{0} | U^\dagger M U | \mathbf{0} \rangle$ .

Zero-noise extrapolation (ZNE) [14, 11] is arguably the simplest of the QEM schemes. Though the noise in a circuit cannot be arbitrarily reduced, it can be increased by various means, such as by adjusting the parameters of a physical device [11, 24], or by circuit folding [25]. Therefore ZNE consists of two main steps: First, the natural error rate of the circuit,  $\varepsilon$ , is boosted at different rates  $\alpha_1, \alpha_2, \dots, \alpha_n$  satisfying  $1 = \alpha_0 < \alpha_1 < \dots < \alpha_n$  to measure expectation values  $\{\langle M \rangle(\alpha_i \varepsilon)\}_{i=0}^n$ . Here  $\langle M \rangle(\varepsilon')$  refers to the expectation value of  $M$  when the error rate of the circuit is  $\varepsilon'$ . Then, these measurement results are extrapolated to the zero-error limit  $\langle M \rangle(0)$  by fitting to a function presumed to describe the behaviour of the circuit under varying rates of noise. Potential fits include Richardson extrapolation [11, 14], a type of polynomial fit where the degree of the fitting polynomial is always equal to the number of data points and exponential extrapolation [12], which is potentially more accurate for deeper circuits [10].

### 2.1.3 Recompilation with ISL

As an alternative to error mitigation, we apply ISL to the Trotter circuits  $\{T^n\}_{n=1}^{N_T}$ , as has been done in previous work [20]. Given  $V_n | \mathbf{0} \rangle \approx T^n | \mathbf{0} \rangle$ , ISL can be used to find a variational circuit  $V_{n+1}$  such that  $V_{n+1} | \mathbf{0} \rangle \approx T V_n | \mathbf{0} \rangle$ . In this manner, the previously optimized variational circuit acts as the new target circuit for the next time step. This is repeated for all  $n = 0, 1, \dots, N_T - 1$ , where  $T^0$  is defined to be the initial state preparation circuit  $U_{\text{st}}$ . The motivation for this recursive approach is that the depth of the executable circuits can be reduced such that they are manageable for noisy devices.

ISL builds the ansatz circuit  $V(\boldsymbol{\theta})$  by appending CNOT gates surrounded by rotation gates to it, attempting to minimize the cost function  $C(\boldsymbol{\theta}) = 1 - |\langle \mathbf{0} | V(\boldsymbol{\theta})^\dagger U | \mathbf{0} \rangle|^2$ . The final cost  $C$  is repeatedly compared to the sufficient cost, denoted by  $C_{\text{suff}}$ . If  $C \leq C_{\text{suff}}$ , the constructed ansatz is acceptable and optimization will terminate, but otherwise another CNOT layer must be added. A more in-depth description of ISL can be found in Appendix A.

ISL has been applied to dynamical mean-field theory [16], time-evolution problems [20, 26], as well as quantum machine learning [27]. Though it is able to reduce circuit depth, its main

drawback is the increased number of circuit evaluations [20].

## 2.2 Model Hamiltonian

Various spin-boson models have been used as model Hamiltonians for demonstrating and investigating quantum algorithms for time-evolution [28, 20, 19, 29]. The model system for the simulations here is chosen to be the Tavis–Cummings model (TCM), the  $N$ -atom generalisation of the Jaynes–Cummings model [30]. The TCM describes  $N$  two-level atoms coupled equally to a quantized electromagnetic field, and its Hamiltonian can be written as [31]

$$\mathcal{H}_{\text{TC}} = \hbar\omega a^\dagger a + \hbar\Omega \sum_{i=1}^N \frac{\sigma_z^{(i)}}{2} + \hbar g \sum_{i=1}^N \left( a\sigma_+^{(i)} + a^\dagger\sigma_-^{(i)} \right). \quad (2)$$

Here  $\omega$  is the frequency of the field mode,  $\hbar\Omega$  is the separation between the atoms' energy levels, and  $g$  is the coupling constant.  $a^{(\dagger)}$  is the annihilation (creation) operator for the bosonic mode, and the Pauli operators  $\{\sigma_\alpha^{(i)} \mid \alpha \in \{x, y, z\}\}$  act on the atoms  $i = 1, \dots, N$ . The spin raising (+) and lowering (−) operators are defined as  $\sigma_\pm^{(i)} \equiv (\sigma_x^{(i)} \pm i\sigma_y^{(i)})/2$ .

For the simulations, we assume  $\hbar = 1$  for simplicity,  $g = 10$ , and that the system is in resonance with  $\Omega = \omega = 1$ . With these assumptions the system Hamiltonian is

$$\mathcal{H} = \omega a^\dagger a + \omega \sum_{i=1}^N \frac{\sigma_z^{(i)}}{2} + g \sum_{i=1}^N \left( a\sigma_+^{(i)} + a^\dagger\sigma_-^{(i)} \right). \quad (3)$$

The initial state is taken to be  $|\psi_0\rangle \equiv |1\rangle \otimes_{i=1}^N |g\rangle_i$ , that is, the field is excited with one photon while all atoms are in their ground states.

### 2.2.1 Qubit encoding

The system Hamiltonian must be mapped into a qubit Hamiltonian for the time-evolution algorithms. The spin- $\frac{1}{2}$  degrees of freedom can be directly associated with qubits such that  $|g\rangle_i = |1\rangle_i$ ,  $|e\rangle_i = |0\rangle_i$ , and the  $\sigma_\alpha^{(i)}$  operators are the Pauli gates. To represent the bosonic Fock states  $|n\rangle$  on a qubit-based quantum computer, we follow the procedure from Ref. [32]. First, the occupation number is truncated to  $D$  levels such that  $0 \leq n < D$ . Since  $|\psi_0\rangle$  has one excitation and the TCM conserves excitations, the occupation number can be truncated to  $D = 2$  values ( $|0\rangle$  and  $|1\rangle$ ) and one qubit is enough to represent the bosonic state. Each occupation number  $n$  is then mapped into a binary string according to some binary encoding  $f$ . Here the encoding is simply  $f(0) = 0$  and  $f(1) = 1$ . The final qubit-encoded Hamiltonian is

$$H = \frac{\omega}{2} \left( \mathbb{I} - \sigma_z^{(0)} \right) + \frac{\omega}{2} \sum_{i=1}^N \sigma_z^{(i)} + \frac{g}{2} \sum_{i=1}^N \left( \sigma_x^{(0)}\sigma_x^{(i)} - \sigma_y^{(0)}\sigma_y^{(i)} \right), \quad (4)$$

requiring  $N_q \equiv N + 1$  qubits. Here the 0th qubit is the encoded bosonic state. The corresponding initial state is  $|\phi_0\rangle = \otimes_{i=0}^{N_q-1} |1\rangle_i$ , prepared by the circuit  $U_{\text{st}} \equiv \otimes_{i=0}^{N_q-1} \sigma_x^{(i)}$ .

## 2.3 Simulations

Starting from the initial state  $|\phi_0\rangle$ , we simulate the qubit-encoded TCM (4) for  $N_T = 20$  time steps with a step size  $\Delta t = 0.01$ . Its Trotter step can be written as

$$T = e^{-i\omega\Delta t/2} \left( R_z^{(0)}(-\omega\Delta t) \prod_{j=1}^N R_z^{(j)}(\omega\Delta t) \right) \left( \prod_{j=1}^N R_{xx}^{(0,j)}(g\Delta t) R_{yy}^{(0,j)}(-g\Delta t) \right), \quad (5)$$

where  $R_{\alpha\alpha}^{(j,k)}(\theta) \equiv \exp(-i\frac{\theta}{2}\sigma_{\alpha}^{(j)} \otimes \sigma_{\alpha}^{(k)})$ . The phase coefficient,  $\exp(-i\omega\Delta t/2)$ , does not affect the probabilities and can be ignored in the circuit implementations.

The time-evolution circuits must be prepended with the initial state preparation circuit, therefore the state of the system after the  $n$ th time step is  $|\varphi(n\Delta t)\rangle \approx T^n U_{\text{st}} |\mathbf{0}\rangle$ . Throughout the simulation we track the probability of observing the initial state,  $\mathbb{P}(|\varphi_0\rangle) \equiv |\langle\varphi_0|\tilde{\varphi}\rangle|^2$ , where  $|\tilde{\varphi}\rangle$  is a state of the system obtained through Trotterization or the other means described above. A probability value instead of fidelity is chosen as the overall metric for comparison since ZNE only mitigates expectation values. However, the fidelities of states obtained with noisy Trotterization and ISL with respect to the ideal, noiseless Trotterization can be and are compared in the results (Section 3.1.1).

The time-evolution circuits were not executed on a quantum device, but instead simulated classically with Qiskit, while the Mitiq [33] package was used for error mitigation. Much of the code used is available on GitHub [34]. The noise model used for the Qiskit simulations is based on `ibm_nairobi`, a seven qubit IBM device [35]. The basis gate set of this device,  $\{\mathbb{I}, R_z, \sqrt{\sigma_x}, \sigma_x, \text{CNOT}\}$ , included in the fake device backend in Qiskit, was also used in the simulations. At the time of choosing this noise model `ibm_nairobi` was still publicly available through the IBM Quantum Platform, however, as of November 2023, the system has been retired [36].

As elaborated above, we investigate the performance of three varieties of time-evolution algorithms: Trotterization, Trotterization with ZNE, and Trotter circuits which have been recompiled with ISL. For each case, we consider a TCM with three different system sizes, as shown in Table 1. Shown in the table is also how the number of shots per each circuit evaluation is also varied during non-error-mitigated Trotterization and ISL, allowing us to tune the total number of circuit evaluations. Since ZNE is known to increase the shot noise associated with circuit evaluation [10], i.e. the variance of the measured expectation value is increased, we instead use  $k = 2^{14} = 16\,384$  shots for all ZNE runs.

$N$	$C_{\text{suff}}$	$k$
1	$10^{-2}$	$2^{10} = 1\,024$
2		$2^{12} = 4\,096$
3	$10^{-4}$	$2^{13} = 8\,192$

Table 1: All parameter values used for the simulations of ISL and Trotterization without ZNE. Here  $N$  is the number of two-level systems in the Tavis–Cummings Hamiltonian,  $C_{\text{suff}}$  is the sufficient cost, i.e. the termination cost of ISL, and  $k$  is the number of shots taken for each circuit execution. Trotterization with ZNE was executed for  $N = 1, 2, 3$  system sizes as well, but with a fixed amount of shots,  $k = 2^{14} = 16\,384$ .

## 2.4 Estimating required circuit evaluations

In the NISQ era, circuits must maintain a sufficiently low depth to be usable, but an algorithm which uses low-depth circuits can still be impractical if the number of required circuit evaluations is large: A quantum algorithm which requires a number of circuit evaluations exponential in  $N_q$

has no advantage over classical ones. The total number of circuit evaluations, denoted here by  $c$ , is therefore an important metric for quantum algorithms.

We consider Trotterized time-evolution first and ISL second. Since we are measuring the probability of a state with  $k$  circuit measurements (i.e. shots) per Trotter step, the number of circuit evaluations is simply

$$c_{\text{Trotter}} = k, \quad (6)$$

ZNE with 3 measurement points increases the evaluation count to

$$c_{\text{Trotter}}^{(\text{ZNE})} = 3k. \quad (7)$$

The total number of evaluations for Trotterization with and without error-mitigation can be found by simply multiplying  $c_{\text{Trotter}}$  and  $c_{\text{Trotter}}^{(\text{ZNE})}$  with the number of Trotter steps.

Previous work [20] has estimated the total circuit evaluations of ISL based on the number of cost function evaluations. However, the authors do not take into account the circuit evaluations required for QST, which is performed for each layer of the circuit. QST estimates the density matrix of the  $N_q$ -qubit system, and requires  $3^{N_q}$  different measurement circuits [37]. The scaling is exponential, but in ISL only qubit pairs are evaluated with QST, and the process only adds a constant 9 measurement circuits per pair. Assuming the worst-case scenario of all-to-all connectivity, the number of qubit pairs to be evaluated is  $N_{qp} = \binom{N_q}{2} = N_q(N_q - 1)/2$ . Therefore the tomography contributes at most a polynomial cost of  $9N_{qp}k = O(N_q^2)$  circuit evaluations per layer. Based on the above, an estimate for the number of circuit evaluations done by ISL is

$$c_{\text{ISL}} \approx k + N_{ce}k + 9N_lN_{qp}k, \quad (8)$$

where  $N_{ce}$  is the number of cost function evaluations,  $N_l$  is the number of layers in the ISL circuit,  $N_{qp}$  is the number of qubit pairs in the coupling map of the device, and  $k$  is the number of shots per circuit evaluation. Increasing  $k$  can only be expected to reduce the shot noise of Trotterization, while increasing  $c_{\text{Trotter}}$  linearly. However, this does not take into account the fact that larger systems will require more shots, since increasing the system size increases the number of qubits, which in turn increases the number of possible states and hence statistical error. Therefore achieving similar measurement accuracies for larger  $N_q$  requires higher  $k$ .

For ISL, the reduced shot noise may also affect  $N_{ce}$  and  $N_l$ , possibly resulting in non-linear scaling. This could allow for more accurate optimization, which could reduce  $N_l$ , as sufficient circuits are reached with less iterations. The effect on  $N_{ce}$  is likely more subtle, as  $k$  increases the number of evaluations, but reduced  $N_l$  could bring the total number down.

As  $N_{ce}$  and  $N_l$  can only be determined after running ISL by seeing the amount of cost function calls made by the algorithm and the number of iterations, neither the resource usage nor the accuracy of the algorithm can be guaranteed beforehand, which is a downside of VQAs in general.

### 3 Results

This section presents and evaluates the results obtained from the simulated time-evolution algorithms. Throughout the following text, *plain* Trotterization refers to the Trotter circuits being simulated as-is under the specified noise model, *ZNE* is the addition of ZNE on top of this, and *ISL* is the recompilation of the Trotter circuits, the algorithm again simulated with noise to mimic execution on a real device. *Exact* refers to ideal simulations of Trotterization without noise. The error caused by the Trotterization itself is therefore not considered here.

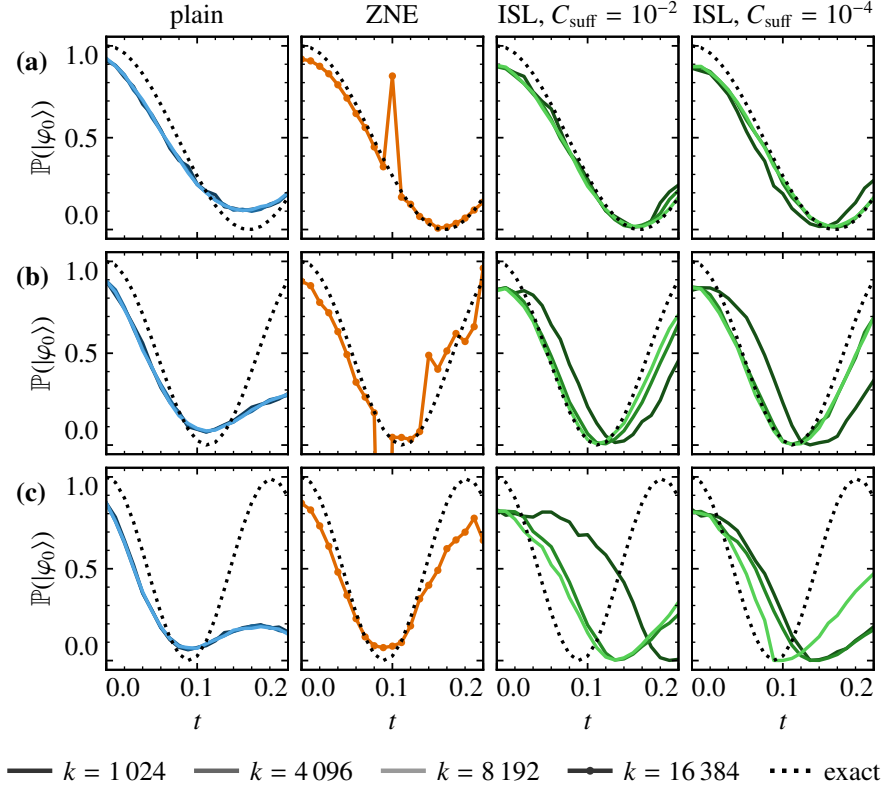


Figure 1: Time-evolution of  $\mathbb{P}(|\varphi_0\rangle)$  for various methods, with system size (a)  $N = 1$ , (b)  $N = 2$ , and (c)  $N = 3$ . *Plain* refers to the plain Trotterization, with other columns signifying the methods used to improve on it, while *exact* is the Trotterized time-evolution without noise. Lighter shades correspond to more shots taken, except for the ZNE curves.

### 3.1 Evolution of probabilities

The time-evolutions of  $\mathbb{P}(|\varphi_0\rangle)$  obtained from the simulations are presented in Fig. 1, with the corresponding absolute error between the measured probabilities and the exact one,  $\varepsilon$ , shown in Fig. 2. The median error over all time steps,  $\tilde{\varepsilon}$ , is shown in Fig. 3. Median error was chosen here instead of average so that individual, erroneous points would not affect the evaluation as much.

The plain Trotterization sets the baseline performance for the simulation, and it particularly struggles to reach the second peak of the exact probability curves due to noise, visible in the larger systems with  $N = 2$  and  $N = 3$ . Trotterization with ZNE is able to lift the probability back to more accurate values, but the extrapolation is unpredictable and at times results in values outside the acceptable  $[0, 1]$ -range (See Fig. 1(b)). Increasing  $k$  has no notable effect on  $\varepsilon$ , as seen in the first column of Fig. 2, therefore e.g. the decoherence of the qubits included in the noise model dominates over shot noise.

ISL was performed for  $C_{\text{suff}} = 10^{-2}$  and  $C_{\text{suff}} = 10^{-4}$ , but the latter does not produce improved results as can be seen in Fig. 3, because the noisy cost function never reaches such low values. Instead the relevant termination criterion for ISL was the cost improvement tolerance, which terminates the optimization once the cost evolution plateaus. This behaviour is visible in Fig. 4, which shows the layer-by-layer cost evolution of the ISL ansätze for the  $k = 2^{13} = 8192$  runs.

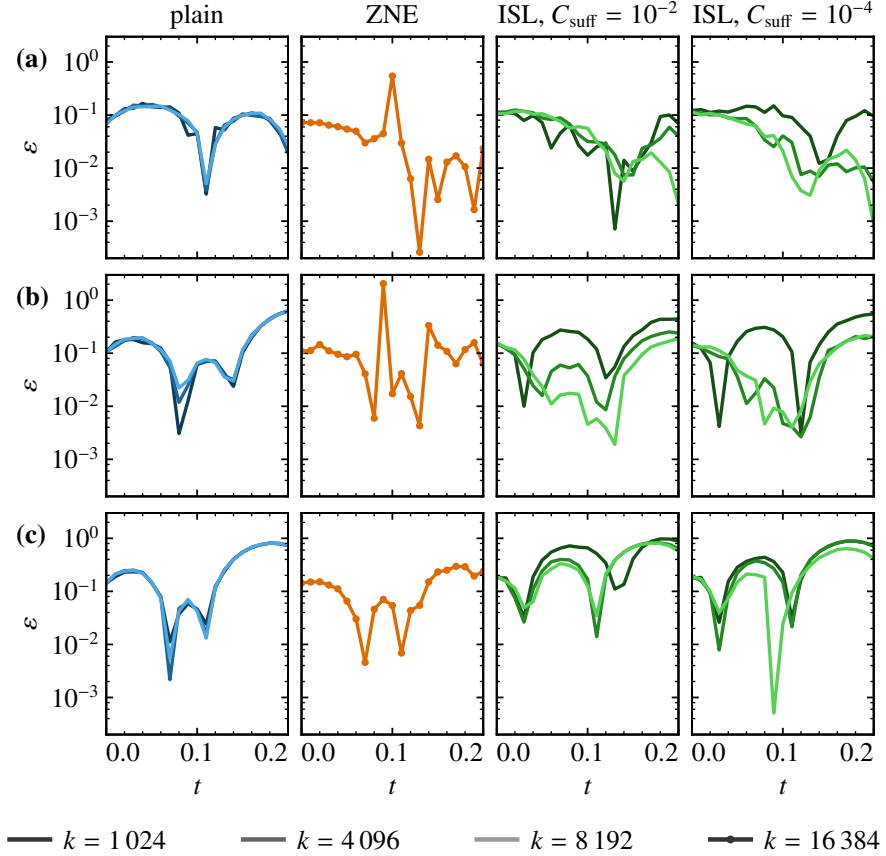


Figure 2: Time-evolution of  $\varepsilon$ — the absolute error in  $\mathbb{P}(|\varphi_0\rangle)$ —for the examined methods with system size (a)  $N = 1$ , (b)  $N = 2$ , and (c)  $N = 3$ .

Strictly speaking, the cost evolution does not completely plateau, rather it slowly drifts back up after reaching a minimum. This is likely explained by the accumulation of noise and approximation error with every layer.

Increasing  $k$  for ISL does improve the results: For  $N = 2$ , the ISL curves lag behind the ideal probability, which is corrected for larger  $k$  (Fig. 1), and as a result the median error of the simulation is pushed down in Fig. 3. This is due to the reduced shot noise allowing for more accurate estimates of expectation values, leading to better optimization of the ansatz variables. However, even with  $k = 2^{13} = 8\,192$  shots, ISL fails for  $N = 3$ , as there is notable lag and distortion visible in Fig. 1. Further increasing the shots to  $k = 2^{14} = 16\,384$ , for example, could improve the lag here as well, but this does not bode well for the scaling of the method.

It is interesting that for the system at play, the error from ISL appears quite consistently either as a lead (Fig. 1(a)) or a lag (Fig. 1(b) and (c)). This is likely a property of the TCM rather than ISL specifically, in the sense that small deviations in the initial state  $|\psi_0\rangle$  correspond to small deviations in the resultant time-evolution.

In summary, for  $N = 1$  and  $N = 2$  the ISL algorithm performs well and is able to reach the lowest median errors, while for  $N = 3$ , ISL fails and the lowest median error is reached with ZNE (Fig. 3).

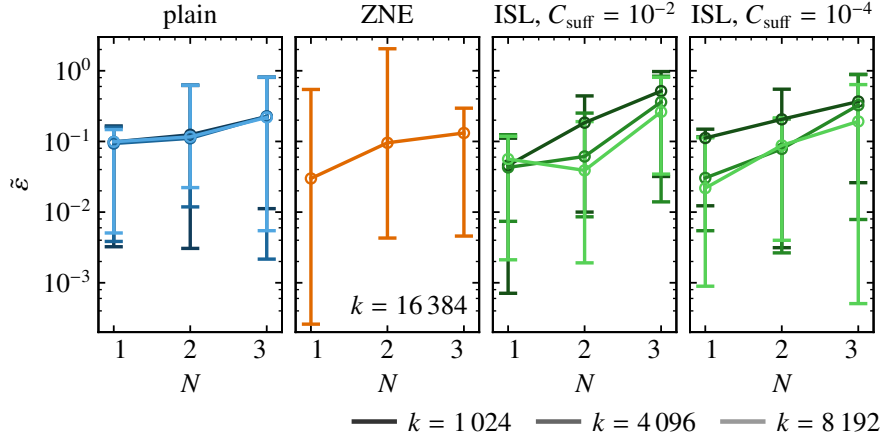


Figure 3: Median of the absolute error over all time steps,  $\tilde{\epsilon}$ , as a function of system size  $N$ . The vertical bars denote minimum and maximum error across the steps.

### 3.1.1 Recompiled fidelities

As an aside, we may also compare the fidelities of plain Trotterization and ISL with respect to the exact, noiseless Trotterization. Comparison for ZNE is not possible, as the method only mitigates expectation values. Fig. 5 shows how the state fidelities evolve as the simulation steps proceed, with the plain Trotterization curves decaying very cleanly due to the noise being artificial. We can see that the ISL time-evolution that achieved the smallest median error for  $N = 2$  corresponds to fidelities of roughly 0.9–0.95 throughout the simulation (Fig. 5(b)). In contrast to this, the fidelities for  $N = 3$  decay almost as quickly or even quicker than the plain case (Fig. 5(c)), with the exception of  $C_{\text{suff}} = 10^{-4}$  and  $k = 2^{13} = 8192$  shots, which finishes around  $F \approx 0.5$ . However, it is clear from Fig. 4 that this is not because of the lower cost being reached, and must have happened simply by chance and the classical optimizer luckily avoiding some less optimal local minimum. This suggests that improvements in the classical optimizer routine could improve the ISL performance, for example by employing methods designed for escaping local minima in the context of VQAs [38]. This would of course add to the current circuit evaluation overhead, which is evaluated in the following section.

## 3.2 Resource requirements

Fig. 6 presents the relationships between the median error  $\tilde{\epsilon}$ , the final depth of the time-evolution circuit i.e. depth required for  $t = 0.2$ , and the combined circuit evaluations of all time steps,  $c$ , for different methods. Even though in principle the circuit depth achieved with ISL could vary from one time step to another, in these simulations the ISL depths remained roughly constant throughout the time steps, and hence the final depth is representative. The circuit depth, i.e. the length of the longest path in the circuit, is in terms of the `ibm_nairobi` basis gates, as this is the depth that would occur during actual execution, and the depth for the ZNE method is taken to be the length of the deepest folded circuit, in this case equal to three times the plain depth. Though ZNE does result in the deepest circuits for execution, this must be evaluated with the knowledge that deeper circuits are necessary for the chosen noise amplification method of circuit folding. ISL depth grows with  $N$  (see Fig. 10 in Appendix B), but remains an order of magnitude lower than

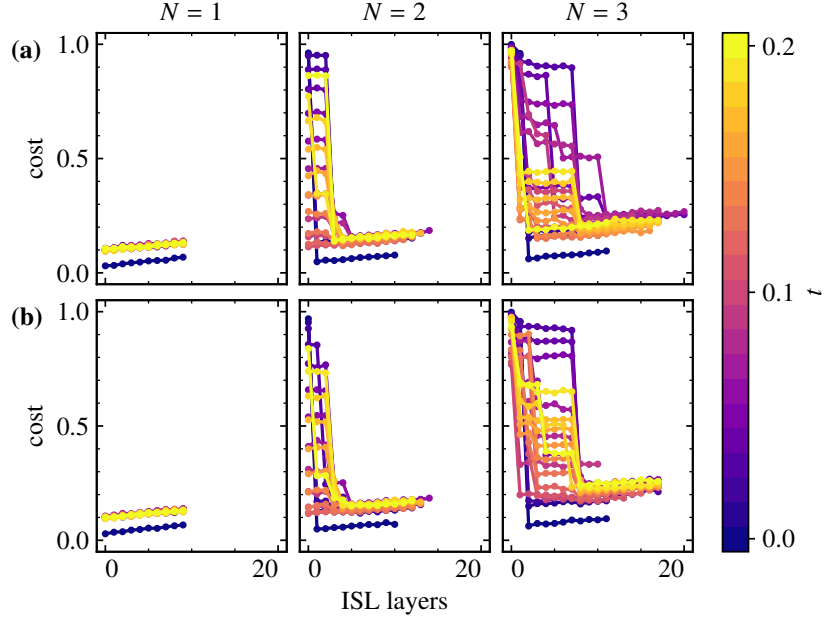


Figure 4: The optimized cost during ISL at the end of each nested CNOT layer for the  $k = 2^{13} = 8192$  shot runs. The rows correspond to (a)  $C_{\text{suff}} = 10^{-2}$  and (b)  $C_{\text{suff}} = 10^{-4}$ . The color of the plot signifies the corresponding time step.

the other methods. However, since ISL failed for  $N = 3$ , the circuit depth required for an accurate recompilation of the  $N \geq 3$  systems could be notably more. Little difference is seen between the different  $C_{\text{suff}}$  values for ISL in terms of circuit depth or evaluations, again due to this termination condition not being triggered.

While ISL does keep the circuit depth low, it requires significantly more circuit evaluations, with the most accurate ISL recompilation of the  $N = 2$  system requiring three orders of magnitude more circuit evaluations than ZNE (Fig. 6(b)). Like with circuit depth, the actual evaluations that an adequate ISL recompilation requires for  $N \geq 3$  could be higher. In general, Fig. 6 shows diverging resource requirements for the ISL and non-ISL based methods, reaffirming the previously mentioned trade-off nature of ISL: a reduction in depth is achieved at a potentially high cost of increased circuit evaluations. This high cost was also noted by Fitzpatrick et al. [20] when comparing ISL to Trotterization and VQS. While increasing the number of circuit evaluations might be an easy way of improving the results for smaller systems, the long-term scaling of the method is important to consider.

### 3.3 Optimal method and future work

As stated previously, the lowest median error is reached by ISL for  $N = 1$  and  $N = 2$ , and by ZNE for  $N = 3$  where ISL fails to reproduce correct dynamics. Taking into account the high cost of circuit evaluations incurred by ISL, and the fact that the deeper circuit depth of ZNE is an artefact of circuit folding, ZNE can be considered the optimal method of the ones evaluated here. While the number of circuit evaluations was manageable for these small system sizes, in larger systems the evaluation cost could render even a low-depth algorithm unusable, as noted in

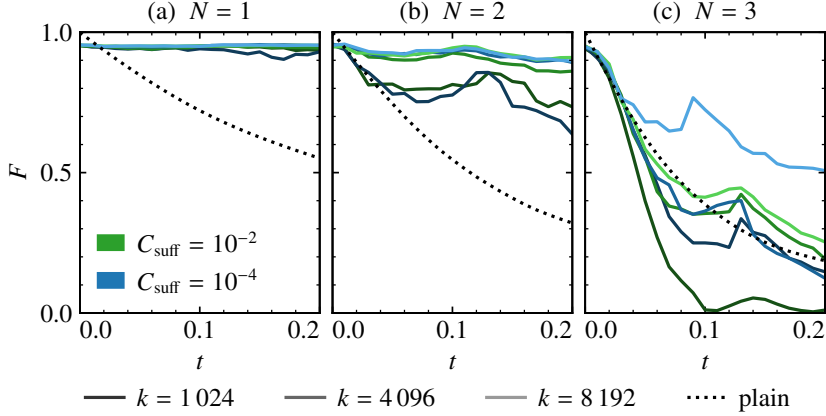


Figure 5: Fidelities of the states,  $F$ , compared to noiseless Trotterization as a function of simulation time. The coloured lines correspond to states obtained through ISL with  $C_{\text{ suff}} = 10^{-2}$  (green) and  $C_{\text{ suff}} = 10^{-4}$  (blue), while the dotted line shows fidelities obtained from the noisy Trotterization.

Ref. [19]. The aforementioned work extrapolates the scaling of VQS and concludes that in its current form it is unlikely to achieve quantum advantage due to the sheer time associated with circuit evaluations. Similar scaling predictions cannot be made for ISL here since the method failed to produce adequate time-evolution for  $N = 3$  and therefore extrapolating either the circuit evaluations or the final depth for  $N > 3$  would be of little use, and even if this was not the case, the number of points for the extrapolation would be quite small.

The typical reason for the termination of ISL appears to have been the plateauing of the cost improvement. This could be improved by increasing the cost improvement tolerance of the algorithm in case the optimizer keeps getting stuck in local minima, likely at the cost of optimization time i.e. circuit evaluations. Regardless of this the difficulty of the classical optimization task will inevitably increase as  $N_q$  and hence the ansatz grows. An interesting question is if ISL and ZNE could be combined in some manner. Fig. 7 shows mitigated probabilities of the  $k = 8192$  ISL runs, mitigated with  $k = 16384$  shots. Little difference is visible between the mitigated and unmitigated probabilities — probably due to the ISL circuits being too short for noise to have a significant effect — confirming that it is the structure and parameters of the  $N = 3$  circuits which are insufficient. Trying to error mitigate the cost function evaluations during ISL iterations with ZNE is questionable due to unpredictability of the extrapolation, but could be better applicable to the QST parts.

Another attempt to improve the ISL procedure would be to use either shorter or longer circuit segments in the recursive recompilation. The longer the segments, the more degraded their final states will be, but the shorter they are, the more approximation error ISL will accumulate throughout the segments. It is not a given that the optimal trade-off between these effects is obtained by segmenting the time-evolution circuit into single, whole Trotter steps.

The QEM method used here also has room for improvement, since ZNE with circuit folding as the noise amplification method is a fairly simple approach to error mitigation. Recently, an IBM team argued to have obtained accurate expectation values from classically intractable time-evolution circuits on a 127-qubit device by using a PEC-based method to amplify errors instead of cancelling them [21], in a way combining PEC and ZNE. A more advanced noise amplification

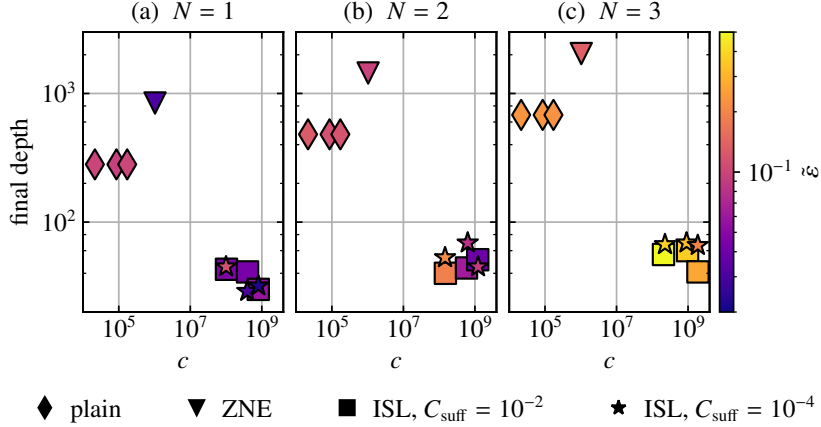


Figure 6: Final circuit depth, total circuit evaluations  $c$ , and the median error in probability  $\tilde{\varepsilon}$ . The subplots correspond to system sizes (a)  $N = 1$ , (b)  $N = 2$ , and (c)  $N = 3$ .

like this could perhaps reduce some the unpredictability of the extrapolation that occurred here.

Limitations of this work include that the dynamics of only a single, specific system were studied, as well as the use of a simulated noise model instead of an authentic device. With  $N_q = 7$  qubits in the model device, simulations could potentially have been done for system sizes up to  $N = 6$ . Here  $N$  was capped at  $N = 3$  due to the long simulation times required by the ISL algorithm, the longest ISL runs requiring approximately 42 hours. Readout error mitigation could have improved the results of all simulations, but was not used here.

## 4 Conclusions

In this work the performance of Trotterized time-evolution of the Tavis–Cum-mings model under simulated noise was compared to two methods which promise improvement for NISQ devices: ZNE with noise amplification by circuit folding, and a variational circuit recompiling algorithm, ISL. Comparison was done for different parameters of system size  $N$ , termination cost of ISL,  $C_{\text{ suff}}$ , and shots used per circuit,  $k$ .

While ISL achieved the lowest median error and high fidelities for the smaller system sizes of  $N = 1$  and  $N = 2$ , it failed to reproduce accurate dynamics for  $N = 3$ , i.e.  $N_q = 4$  qubits. This was due to the plateauing of cost improvement, which terminates the classical optimization routine. Though ZNE was able to improve the noisy Trotterization, its main hindrance was the unpredictability of the extrapolation, leading to erroneous outlier points. The circuit depth of ISL remained small as opposed to the linearly growing depth required by ZNE, but the number of circuit evaluations was consistently at least two orders of magnitude higher than for ZNE. In this manner the methods showed diverging resource requirements.

Improvements that could be considered for ISL include increasing or decreasing the length of the circuit segments used in the recursive recompilation. Shorter segments could make the optimization task of each step easier, while longer segments could reduce the error from recursion, and the optimal balance between these two effects could be considered. Taking advantage of features specific to cost functions of VQAs could improve the classical optimization part [38].

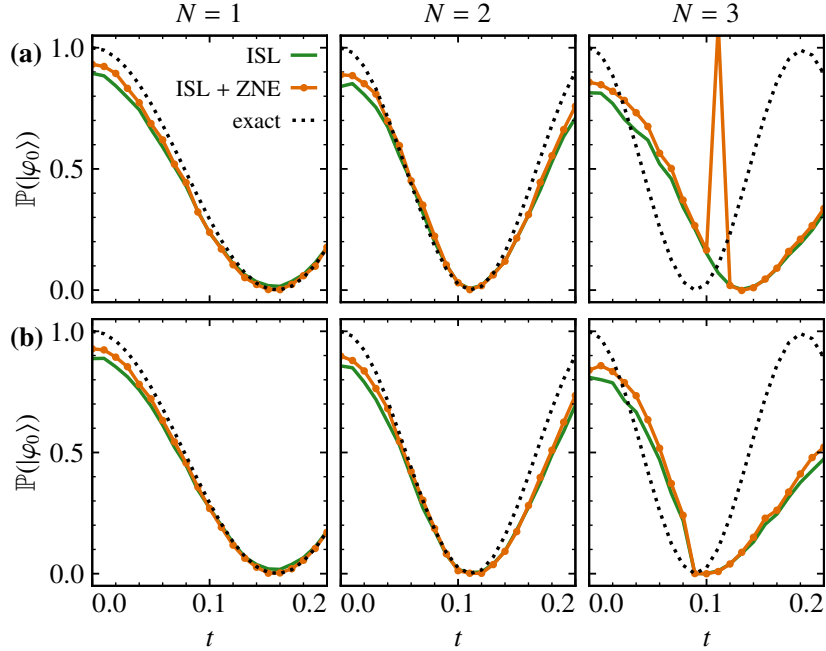


Figure 7: Time-evolution circuits obtained through ISL with  $k = 8192$  shots are rerun and error-mitigated with ZNE and  $k = 16384$  shots. The sufficient cost is (a)  $C_{\text{suff}} = 10^{-2}$  and (b)  $C_{\text{suff}} = 10^{-4}$ .

Refining the classical optimization routines of VQAs overall is of importance if they are to be candidates for quantum advantage. Additionally, implementing QEM in the qubit pair tomography part of the algorithm could improve ansatz construction. ZNE in its form here is likely too unstable to work reliably, but a more involved method of noise amplification, such as Pauli twirling [14], or a wholly different QEM method such as PEC, could perhaps be applied to the cost evaluation parts as well. While they add evaluation overhead, they could also hasten the optimization by facilitating more accurate measurements of expectation values. Of course these changes could also be applied by themselves to better or replace ZNE. As the simulated systems grow larger, choosing the optimal qubit encoding will also be important [39, 32].

To our knowledge, recursive recompilation of Trotter circuits with ISL, where the circuits are run with noise during the optimization itself has not been reported on previously, and the challenges that ISL faced here with small systems of 4 qubits show that further work is required before the method can be extended to larger systems on NISQ devices.

## 5 Acknowledgments

Funding for this work was provided by Business Finland project 8726/31/2022 “Computational interfaces between classical data and quantum computing units for practical near-term applications of quantum machine learning (CICAQU)”. The authors acknowledge the computational resources provided by the Aalto University School of Science “Science-IT” project.

## References

- [1] Bela Bauer, Sergey Bravyi, Mario Motta, and Garnet Kin-Lic Chan. Quantum algorithms for quantum chemistry and quantum materials science. *Chemical Reviews*, **120**:12685–12717, 2020. arXiv:2001.03685.
- [2] Lindsay Bassman, Miroslav Urbanek, Mekena Metcalf, et al. Simulating quantum materials with digital quantum computers. *Quantum Science and Technology*, **6**:043002, 2021. arXiv:2101.08836.
- [3] Tim Byrnes and Yoshihisa Yamamoto. Simulating lattice gauge theories on a quantum computer. *Physical Review A*, **73**:022328, 2006. arXiv:quant-ph/0510027.
- [4] Richard P. Feynman. Simulating physics with computers. *International Journal of Theoretical Physics*, **21**:467–488, 1982.
- [5] Seth Lloyd. Universal quantum simulators. *Science*, **273**:1073–1078, 1996.
- [6] H. F. Trotter. On the product of semi-groups of operators. *Proceedings of the American Mathematical Society*, **10**:545–551, 1959.
- [7] Michael A. Nielsen and Isaac L. Chuang. *Quantum Computation and Quantum Information*. Cambridge University Press, 2010.
- [8] I. M. Georgescu, S. Ashhab, and Franco Nori. Quantum simulation. *Reviews of Modern Physics*, **86**:153–185, 2014. arXiv:1308.6253.
- [9] John Preskill. Quantum computing in the NISQ era and beyond. *Quantum*, **2**:79, 2018. arXiv:1801.00862.
- [10] Suguru Endo, Zhenyu Cai, Simon C. Benjamin, and Xiao Yuan. Hybrid quantum-classical algorithms and quantum error mitigation. *Journal of the Physical Society of Japan*, **90**:032001, 2021. arXiv:2011.01382.
- [11] Kristan Temme, Sergey Bravyi, and Jay M. Gambetta. Error mitigation for short-depth quantum circuits. *Physical Review Letters*, **119**:180509, 2017. arXiv:1612.02058.
- [12] Suguru Endo, Simon C. Benjamin, and Ying Li. Practical quantum error mitigation for near-future applications. *Physical Review X*, **8**:031027, 2018. arXiv:1712.09271.
- [13] M. Cerezo, Andrew Arrasmith, Ryan Babbush, et al. Variational quantum algorithms. *Nature Reviews Physics*, **3**:625–644, 2021. arXiv:2012.09265.
- [14] Ying Li and Simon C. Benjamin. Efficient variational quantum simulator incorporating active error minimization. *Physical Review X*, **7**:021050, 2017. arXiv:1611.09301.
- [15] Kishor Bharti and Tobias Haug. Quantum assisted simulator. *Physical Review A*, **104**:042418, 2021. arXiv:2011.06911.
- [16] B. Jaderberg, A. Agarwal, K. Leonhardt, M. Kiffner, and D. Jaksch. Minimum hardware requirements for hybrid quantum–classical DMFT. *Quantum Science and Technology*, **5**:034015, 2020. arXiv:2002.04612

- [17] Cristina Cîrstoiu, Zoë Holmes, Joseph Iosue, et al. Variational fast forwarding for quantum simulation beyond the coherence time. *npj Quantum Information*, **6**:1–10, 2020. arXiv:1910.04292.
- [18] Michael Tavis and Frederick W. Cummings. Exact solution for an  $N$ -molecule-radiation-field Hamiltonian. *Physical Review*, **170**:379–384, 1968.
- [19] Alexander Miessen, Pauline J. Ollitrault, and Ivano Tavernelli. Quantum algorithms for quantum dynamics: A performance study on the spin-boson model. *Physical Review Research*, **3**:043212, 2021. arXiv:2108.04258.
- [20] Nathan Fitzpatrick, Harriet Apel, and David Muñoz Ramo. Evaluating low-depth quantum algorithms for time evolution on fermion-boson systems, preprint, 2021. arXiv:2106.03985.
- [21] Youngseok Kim, Andrew Eddins, Sajant Anand, et al. Evidence for the utility of quantum computing before fault tolerance. *Nature*, **618**:500–505, 2023.
- [22] Yuan Su, Hsin-Yuan Huang, and Earl T. Campbell. Nearly tight Trotterization of interacting electrons. *Quantum*, **5**:495, 2021. arXiv:2012.09194.
- [23] J. Han, W. Cai, L. Hu, et al. Experimental simulation of open quantum system dynamics via Trotterization. *Physical Review Letters*, **127**:020504, 2021. arXiv:2108.02395.
- [24] Abhinav Kandala, Kristan Temme, Antonio D. Córcoles, et al. Error mitigation extends the computational reach of a noisy quantum processor. *Nature*, **567**:491–495, 2019. arXiv:1805.04492.
- [25] Tudor Giurgica-Tiron, Yousef Hindy, Ryan LaRose, Andrea Mari, and William J. Zeng. Digital zero noise extrapolation for quantum error mitigation. In *2020 IEEE International Conference on Quantum Computing and Engineering (QCE)*, pages 306–316, 2020. arXiv:2005.10921.
- [26] Ben Jaderberg, Alexander Eisfeld, Dieter Jaksch, and Sarah Mostame. Recompilation-enhanced simulation of electron-phonon dynamics on IBM quantum computers. *New Journal of Physics*, **24**:093017, 2022. arXiv:2202.08270.
- [27] Ben Jaderberg, Lewis W. Anderson, Weidi Xie, et al. Quantum self-supervised learning. *Quantum Sci. Technol.*, **7**:035005, 2022. arXiv:2103.14653.
- [28] Agustin Di Paolo, Panagiotis Kl. Barkoutsos, Ivano Tavernelli, and Alexandre Blais. Variational quantum simulation of ultrastrong light-matter coupling. *Physical Review Research*, **2**:033364, 2020. arXiv:1909.08640.
- [29] Weitang Li, Jiajun Ren, Sainan Huai, et al. Efficient quantum simulation of electron-phonon systems by variational basis state encoder. *Physical Review Research*, **5**:023046, 2023. arXiv:2301.01442.
- [30] E.T. Jaynes and F.W. Cummings. Comparison of quantum and semiclassical radiation theories with application to the beam maser. *Proceedings of the IEEE*, **51**:89–109, 1963.
- [31] Jonas Larson and Themistoklis Mavrogordatos. *The Jaynes–Cummings Model and Its Descendants: Modern research directions*. IOP Publishing, 2021.

- [32] Nicolas P. D. Sawaya, Tim Menke, Thi Ha Kyaw, et al. Resource-efficient digital quantum simulation of d-level systems for photonic, vibrational, and spin-s Hamiltonians. *npj Quantum Information*, **6**:1–13, 2020.
- [33] Ryan LaRose, Andrea Mari, Sarah Kaiser, et al. Mitiq: A software package for error mitigation on noisy quantum computers. *Quantum*, **6**:774, 2022. arXiv:2009.04417.
- [34] Alisa Haukisalmi. Spin-boson simulation. GitHub repository, <https://github.com/ahaukis/spin-boson-sim/>, 2023. [Accessed 2023-12-20].
- [35] IBM Quantum Platform. <https://quantum-computing.ibm.com/>, 2023. [Accessed 2023-11-02].
- [36] IBM Quantum Documentation. Retired systems. <https://docs.quantum.ibm.com/run/retired-systems/>, 2023. [Accessed 2023-12-03].
- [37] Joseph B. Altepeter, Daniel F.V. James, and Paul G. Kwiat. Qubit quantum state tomography. In *Quantum State Estimation*, Lecture Notes in Physics, pages 113–145. Springer, 2004.
- [38] Enrico Fontana, M. Cerezo, Andrew Arrasmith, Ivan Rungger, and Patrick J. Coles. Non-trivial symmetries in quantum landscapes and their resilience to quantum noise. *Quantum*, **6**:804, 2022. arXiv:2011.08763.
- [39] Mark Steudtner and Stephanie Wehner. Fermion-to-qubit mappings with varying resource requirements for quantum simulation. *New Journal of Physics*, **20**:063010, 2018. arXiv:1712.07067.
- [40] William K. Wootters. Entanglement of formation of an arbitrary state of two qubits. *Physical Review Letters*, **80**:2245–2248, 1998. arXiv:quant-ph/9709029.
- [41] Mateusz Ostaszewski, Edward Grant, and Marcello Benedetti. Structure optimization for parameterized quantum circuits. *Quantum*, **5**:391, 2021. arXiv:1905.09692.

## Appendices

### A Incremental structural learning (ISL)

This appendix describes the ISL algorithm in more detail, and is largely based on Ref. [16]. ISL is a method of recompiling circuits layer-by-layer, starting from a fixed initial state  $|\mathbf{0}\rangle \equiv |0\rangle^{\otimes N_q}$ , where  $N_q$  is the number of qubits. To select another initial state, a state preparation circuit can be added to the beginning of the target circuit  $U$ . The target is compiled into a parameterized circuit

$$V(\boldsymbol{\theta}) = V_1(\boldsymbol{\theta}_1)V_2(\boldsymbol{\theta}_2) \cdots V_l(\boldsymbol{\theta}_l), \quad (9)$$

where each layer  $V_i(\boldsymbol{\theta}_i)$  is a nested CNOT gate (see Fig. 8). New layers are added until a convergence criterion is reached, therefore the structure of the ansatz and the size of the parameter vector  $\boldsymbol{\theta}$  change during the procedure.

The cost function that ISL seeks to minimize is

$$C(\boldsymbol{\theta}) = 1 - |\langle \mathbf{0} | V(\boldsymbol{\theta})^\dagger U | \mathbf{0} \rangle|^2, \quad (10)$$

or in other words, it seeks to maximize the fidelity

$$F(V(\boldsymbol{\theta}) | \mathbf{0}, U | \mathbf{0}) = |\langle \mathbf{0} | V(\boldsymbol{\theta})^\dagger U | \mathbf{0} \rangle|^2. \quad (11)$$

The ansatz is built as an adjoint  $V^\dagger$ , with layers appended to the previous state of the cost circuit  $V_l^\dagger V_{l-1}^\dagger \cdots V_1^\dagger U | \mathbf{0} \rangle$  in order to bring it closer to the  $|\mathbf{0}\rangle$  state. Considering an ansatz with  $l$  layers (Eq. (9)), the ISL algorithm for layer  $l+1$  proceeds as follows:

1. A nested CNOT  $V_{l+1}(\boldsymbol{\theta}_{l+1})$  is added between the qubit pair that achieves the highest value for a chosen entanglement measure, such as the entanglement of formation [40], yielding a new ansatz circuit

$$V(\boldsymbol{\theta}) \equiv V_1(\boldsymbol{\theta}_1) \cdots V_l(\boldsymbol{\theta}_l) V_{l+1}(\boldsymbol{\theta}_{l+1}).$$

Evaluating the entanglement measure requires the use of quantum state tomography (QST) to estimate the density matrices between qubit pairs.

As stated, the goal is to evolve the state  $V_l^\dagger V_{l-1}^\dagger \cdots V_1^\dagger U | \mathbf{0} \rangle$  back into  $|\mathbf{0}\rangle$ . Therefore adding  $V_{l+1}^\dagger$  between the most entangled pair of qubits is motivated by an attempt to "untangle" them.

2. The Rotoselect [41] algorithm is applied to the rotation axes and angles of  $V_{l+1}(\boldsymbol{\theta}_{l+1})$  to minimize Eq. (10). Note that all previous axes and angles belonging to  $V_1, V_2, \dots$  and  $V_l$

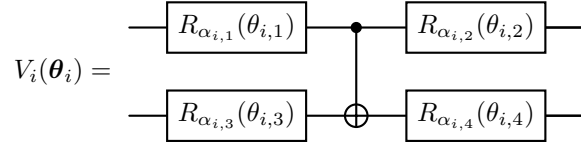


Figure 8: A nested CNOT gate, which is a CNOT surrounded by four single-axis rotation gates. Here  $\boldsymbol{\theta}_i = (\theta_{i,1}, \theta_{i,2}, \theta_{i,3}, \theta_{i,4})$  are the rotation angles and  $\alpha_{i,k} \in \{x, y, z\}$  the rotation axes.

are kept fixed. After this, Eq. (10) is minimized again, this time with the Rotosolve [41] algorithm such that all angles  $\boldsymbol{\theta} = (\boldsymbol{\theta}_1, \boldsymbol{\theta}_2, \dots, \boldsymbol{\theta}_{l+1})$  are allowed to change, but all axes are fixed.

3. Finally, the circuit is simplified appropriately by removing duplicate gates and rotation gates with angles close to zero. A final evaluation of the cost function determines whether to terminate, or to add another layer and continue from the first step.

An illustration of the construction of the ansatz can be seen in Fig. 9.

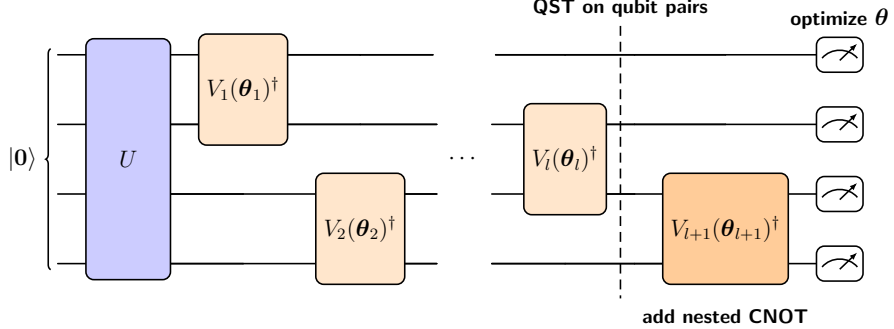


Figure 9: Layer-by-layer construction of the ansatz circuit  $V(\boldsymbol{\theta})$  during ISL. The circuit is initially in the state  $V_l^\dagger V_{l-1}^\dagger \cdots V_1^\dagger U |0\rangle$ . First, state tomography is performed on all qubit pairs to find the most entangled one. A nested CNOT,  $V_{l+1}(\boldsymbol{\theta}_{l+1})^\dagger$ , is appended after this pair, and the circuit parameters are optimized. The optimization may terminate or continue for another layer.

## B Scaling of circuit depth and evaluations

The figures in this appendix show a different view of the circuit depth and evaluations data presented in Fig. 6, instead emphasising the  $N$ -dependence.

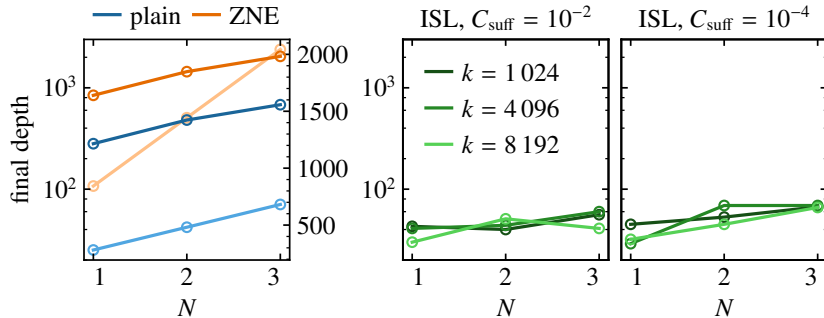


Figure 10: Depth of the final time-evolution circuits achieved by the different methods as functions of system size  $N$ . The lighter curves in the first plot (plain and error-mitigated Trotterization) show the same points on a linear scale.

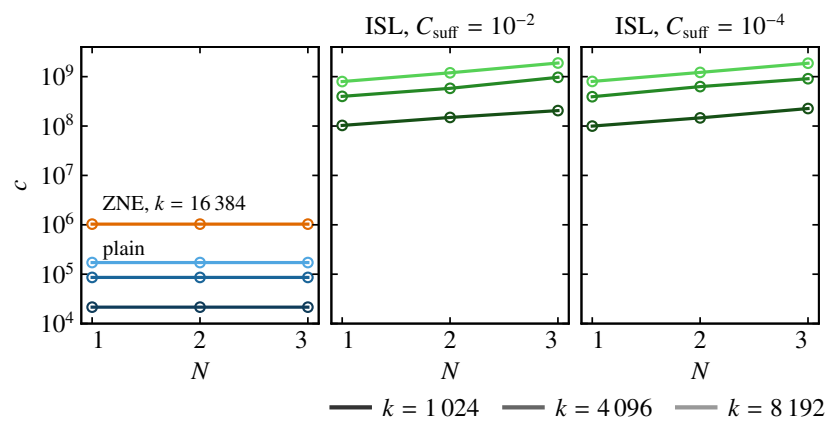


Figure 11: Total circuit evaluations ( $c$ ) done by each method as functions of  $N$ .